International Journal of Physics and Mathematics

E-ISSN: 2664-8644
P-ISSN: 2664-8636
Impact Factor (RJIF): 8.21
IJPM 2026; 8(2): 62-71

www.physicsjournal.net
Received: 14-05-2026
Accepted: 17-06-2026

Gerald Wanjala Chonge
Department of Physics, University Of Eldoret, Eldoret, Kenya

Hezekiah Komen Cherop
Department of Physical, Biological and Health sciences, Rongo University, Rongo, Kenya

Jason Kanule
Department of Physics, University Of Eldoret, Eldoret, Kenya

Corresponding Author:
Gerald Wanjala Chonge
Department of Physics, University Of Eldoret, Eldoret, Kenya

Neutron skin thickness and the transition from cluster decay to spontaneous fission in superheavy nuclei

Gerald Wanjala Chonge, Hezekiah Komen Cherop and Jason Kanule

DOI: https://www.doi.org/10.33545/26648636.2026.v8.i2a.243

Abstract
Understanding the competition between cluster decay and spontaneous fission is essential for elucidating the stability and decay characteristics of neutron-rich superheavy nuclei. In this work, the density-dependent cluster model combined with the Wentzel-Kramers-Brillouin (WKB) approximation is employed to investigate the competing decay modes of selected superheavy nuclei with atomic number Z>103. Cluster-decay penetrabilities, decay constants, together with spontaneous-fission barrier heights and half-lives, are calculated using the AME2020 nuclear mass evaluation and validated against the available experimental data from NUBASE2020.
The calculations demonstrate that cluster decay is governed primarily by decay Q-values, barrier penetrability, shell effects, and daughter-nucleus configurations, whereas spontaneous-fission half-lives decrease systematically with increasing fissility as the calculated fission barriers are reduced. To probe the structural evolution of the investigated isotopic chains, the calculated decay characteristics are further analysed in relation to neutron skin thickness. A transition from cluster-decay dominance to spontaneous-fission dominance is observed for nuclei exhibiting larger neutron skin thickness. The observed trends are consistent with the systematic evolution of nuclear structure and decay energetics across the investigated isotopic chains, with neutron skin thickness serving as a structural indicator rather than an independent driver of the calculated decay properties. Comparison with the available experimental spontaneous-fission half-lives yields a root-mean-square deviation of 1.822, demonstrating satisfactory agreement with experiment. The present study establishes a systematic benchmark for assessing the competition between cluster decay and spontaneous fission in superheavy nuclei and provides a reference for the development and validation of microscopic models incorporating neutron-skin-dependent nuclear interactions.

Keywords: Cluster decay, decay half-lives, fission barrier, neutron skin thickness, Superheavy nuclei

Introduction

Superheavy nuclei (SHN) occupy the uppermost region of the nuclear chart, where nuclear stability arises from the delicate balance between the attractive short-range nuclear force and the increasingly dominant Coulomb repulsion associated with large proton numbers. As the proton number increases, Coulomb repulsion progressively destabilizes the nucleus, leading to rapid radioactive decay. Microscopic shell effects, however, provide additional binding energy that partially counteracts this instability, giving rise to the predicted *island of stability*, where selected superheavy nuclei are expected to exhibit comparatively longer half-lives. The search for this region remains a central objective of contemporary nuclear physics, motivating sustained experimental efforts to synthesize heavier elements and extensive theoretical investigations of their formation, stability, and decay properties [1-4].

Among the principal radioactive-decay modes of heavy and superheavy nuclei, cluster decay and spontaneous fission play a decisive role in determining nuclear stability [5-8]. Their relative probabilities govern the dominant decay pathway and, consequently, the observable lifetime of a nucleus [9-13]. Both processes proceed through quantum tunnelling across finite potential barriers and are therefore highly sensitive to nuclear structure, shell effects, deformation, decay energy, and barrier characteristics [14-17]. A comprehensive understanding of the competition between cluster decay and spontaneous fission is therefore essential for describing the stability of superheavy nuclei and identifying the conditions under which one decay mode becomes dominant [18-23].

Significant progress has been achieved in modelling both cluster decay and spontaneous fission [24-27].

Density-dependent cluster models, microscopic interaction potentials, and refined empirical formulations have substantially improved predictions of cluster-decay half-lives through the incorporation of realistic nuclear densities, interaction potentials, shell effects, and daughter-nucleus deformations [28-30]. Similarly, modern spontaneous-fission models have advanced through the inclusion of shell corrections, multidimensional deformation, pairing correlations, collective inertia, and microscopic energy-density functionals, leading to increasingly reliable predictions of fission barriers and spontaneous-fission half-lives [31]. These developments have demonstrated that the competition between cluster decay and spontaneous fission is strongly influenced by nuclear structure, shell stabilization, and barrier characteristics, emphasizing the importance of treating both decay modes within a consistent theoretical framework [32-34].

In parallel with these developments, neutron skin thickness has emerged as an important indicator of the structure of neutron-rich nuclei. Defined as the difference between the root-mean-square neutron and proton radii, neutron skin thickness reflects the spatial extension of excess neutrons beyond the proton distribution and is closely related to the density dependence of the nuclear symmetry energy [35-37]. Variations in neutron skin thickness modify nuclear surface properties, including the effective nuclear radius, surface diffuseness, and density distribution, thereby influencing interaction barriers and other barrier-dependent nuclear processes. Although its significance for nuclear structure and reaction dynamics has been widely recognized, its relationship with the competition between cluster decay and spontaneous fission remains comparatively unexplored. Existing decay models generally account for neutron-rich effects indirectly through nuclear-density distributions, effective interaction potentials, or isospin-dependent quantities rather than treating neutron skin thickness as an independent model parameter [38-41].

Motivated by this gap, the present study employs the density-dependent cluster model within the Wentzel-Kramers-Brillouin (WKB) approximation to investigate the competition between cluster decay and spontaneous fission in selected superheavy nuclei with atomic number Z>103. Cluster-decay penetrabilities, decay constants, spontaneous-fission barrier heights, and half-lives are calculated using the AME2020 nuclear mass evaluation and assessed against the available experimental data from NUBASE2020 [42, 43]. The calculated decay characteristics are subsequently analysed in relation to neutron skin thickness to identify systematic structural trends across the investigated isotopic chains. Within the present framework, neutron skin thickness is considered a structural indicator of nuclear structure evolution rather than an independent input to the decay model. The present study provides a systematic assessment of the competition between cluster decay and spontaneous fission in superheavy nuclei and establishes benchmark calculations for future theoretical and microscopic investigations of neutron-rich superheavy systems.

Theoretical framework

The competition between cluster decay and spontaneous fission in superheavy nuclei is investigated within the density-dependent cluster model (DDCM) combined with the Wentzel-Kramers-Brillouin (WKB) approximation and is referred to as, conventional approach. The DDCM provides a microscopic description of barrier-penetration processes by incorporating realistic nuclear interaction potentials and density-dependent effects, while the WKB approximation is employed to evaluate the quantum tunnelling probabilities associated with both decay modes. Within this framework, cluster decay is described as the emission of a preformed cluster through the interaction barrier, whereas spontaneous fission is treated as the penetration of the multidimensional fission barrier along the collective deformation coordinate. The theoretical formalism adopted in the present work is summarized below.

i. Cluster Decay Formalism

Within the density-dependent cluster model, the radioactive-decay constant is determined by the combined effects of the cluster preformation probability, assault frequency, and barrier penetrability, and is expressed as [5, 6],

$$\lambda = S_c \nu P \tag{1}$$

where, S_c is the cluster preformation factor, ν is the assault frequency representing the frequency with which the preformed cluster approaches the barrier, and P is the barrier penetrability.

The barrier penetrability is evaluated using the WKB approximation [8-10],

$$P = exp\left[-\frac{2}{\hbar}\int_{r_i}^{r_o} \sqrt{2\mu c^2(V(r)-Q)}\, dr\right] \tag{2}$$

where, μc^2 is the reduced mass of the decay system, $V(r)$ is the total interaction potential, Q is the decay energy obtained from the AME2020 nuclear mass evaluation, r_o is outer classical turning point and r_i is inner classical turning point [8-10].

The corresponding cluster-decay half-life is obtained from,

$$T_{\frac{1}{2}} = \frac{ln2}{\lambda}, \tag{3}$$

which represents the measurable lifetime associated with cluster emission [6].

ii. Spontaneous Fission Formalism

The spontaneous-fission process is described through the deformation-dependent total potential energy, which consists of the surface, Coulomb, symmetry-energy, shell-correction, and pairing-energy contributions [21-23,25],

$$V_{SF}^{(0)}(q) = E_S^{(0)}(q) + E_C^{(0)}(q) + E_{sym}^{(0)}(q) + \delta E_{shell}(q) + \delta E_{pair}(q). \tag{4}$$

The spontaneous-fission barrier height is determined from the difference between the saddle-point and ground-state potential energies,

$$B_f^{(0)} = V_{SF}^{(0)}(q_s) - V_{SF}^{(0)}(q_g) \tag{5}$$

where (q_s) and (q_g) denote the saddle-point and ground-state deformation coordinates, respectively.

The probability of spontaneous-fission barrier penetration is evaluated using the WKB action integral,

$$K_{SF}^{(0)} = -\frac{2}{\hbar}\int_{q_a}^{q_b} \sqrt{2B_{SF}^{(0)}(q)\left[U_{SF}^{(0)}(q) - E_0\right]}\, dq \tag{6}$$

where q_a and q_b are the classical turning points, $B_{SF}^{(0)}(q)$ is the collective inertia (mass parameter), $U_{SF}^{(0)}(q)$ is the deformation-

dependent potential energy, and E_0 is the collective ground-state energy [9-11].
The corresponding spontaneous-fission barrier penetrability is then expressed as,

$$P_{SF}^{(0)} = \left[1 + exp\left(2K_{SF}^{(0)}\right)\right]^{-1}. \quad (7)$$

The spontaneous-fission decay constant is subsequently calculated from the product of the assault frequency and barrier penetrability,

$$\lambda_{SF}^{(0)} = \nu_{SF}^{(0)} P_{SF}^{(0)} \quad (8)$$

where, $\nu_{SF}^{(0)}$ denotes the spontaneous-fission assault frequency. Finally, the spontaneous-fission half-life is obtained from,

$$T_{1/2,SF}^{(0)} = \frac{ln2}{\lambda_{SF}^{(0)}} \quad (9)$$

which represents the characteristic lifetime associated with spontaneous-fission decay [21, 23].

iii. Neutron Skin Thickness

The neutron skin thickness is defined as the difference between the root-mean-square neutron and proton radii,

$$\Delta R_{np} = R_n - R_p \quad (10)$$

where R_n and R_p denote the neutron and proton root-mean-square radii, respectively. In the present study, neutron skin thickness is analyzed as a structural observable to examine systematic variations in the calculated decay characteristics across the investigated isotopic chains. It is not introduced as an independent input parameter to the decay model but is used to assess correlations between nuclear structure and the competing decay modes.

iv. Model Performance

The predictive performance of the theoretical framework is evaluated through the root-mean-square (RMS) deviation between the calculated and available experimental logarithmic half-lives,

$$\sigma_{RMS} = \sqrt{\frac{1}{N}\sum_{i=1}^{N}\left[\log_{10}\left(T_{1/2}^{calc}\right) - \log_{10}\left(T_{1/2}^{exp}\right)\right]^2} \quad (11)$$

where, N is the number of parent nuclei included in the comparison, $T_{1/2}^{calc}$ are the calculated half-lives and $T_{1/2}^{exp}$ the experimental half-lives. Experimental half-lives are taken from the NUBASE2020 evaluation. The RMS deviation provides a quantitative measure of the predictive accuracy of the theoretical framework and serves as the primary metric for assessing agreement with the available experimental data.

Results and Discussion

The decay characteristics of the investigated superheavy nuclei were evaluated using the theoretical framework described in Section 2. Nuclear masses of the parent nuclei, daughter nuclei, emitted clusters, and spontaneous-fission fragments were adopted from the AME2020 nuclear mass evaluation to determine the corresponding decay Q-values. Neutron skin thickness was calculated using Equation (10), while cluster-decay penetrabilities, decay constants, and half-lives were obtained from Equations (2), (1), and (3), respectively. Spontaneous-fission barrier heights, decay propability, and half-lives were evaluated using Equations (5), (9) and (8) respectively. The complete set of calculated decay properties is summarized in Table 1, providing the basis for a systematic assessment of the competition between cluster decay and spontaneous fission across the investigated superheavy isotopic chains.

The calculated decay Q-values exhibit systematic variations across the investigated nuclei, reflecting the evolution of nuclear binding energies with increasing neutron and proton numbers. Similarly, neutron skin thickness increases progressively with neutron excess, consistent with the gradual extension of the neutron density distribution beyond the proton distribution in neutron-rich superheavy nuclei. These structural changes provide an appropriate framework for examining the evolution of the calculated decay characteristics and their relationship to the underlying properties of the nuclear system.

The results presented in Table 1 demonstrate that the calculated cluster-decay characteristics exhibit pronounced but non-monotonic variations throughout the investigated isotopic chains. Such behaviour indicates that cluster decay cannot be interpreted solely in terms of neutron skin thickness. Instead, the calculated penetrabilities, decay constants, and half-lives arise from the combined influence of decay Q-values, interaction-barrier characteristics, shell stabilization, daughter-nucleus configurations, emitted-cluster properties, and the exponential dependence of the tunnelling probability described by the WKB approximation. Consequently, nuclei possessing comparable neutron skin thicknesses may exhibit substantially different cluster-decay half-lives because relatively small variations in decay energy or barrier properties produce significant changes in barrier penetrability and, therefore, in the corresponding decay probability.

In contrast, the spontaneous-fission characteristics display a more systematic evolution across the investigated nuclei. As the proton and mass numbers increase, the calculated spontaneous-fission barrier heights decrease progressively owing to the increasing fissility and enhanced Coulomb repulsion characteristic of heavier superheavy systems. The resulting increase in barrier penetrability produces systematically shorter spontaneous-fission half-lives, indicating that spontaneous fission becomes progressively more competitive as the stabilizing influence of the fission barrier is reduced. This behaviour is consistent with the established dependence of spontaneous-fission probabilities on barrier height and collective tunnelling dynamics.

A comparison of the calculated cluster-decay and spontaneous-fission characteristics reveals a gradual transition from cluster-decay dominance to spontaneous-fission dominance across the investigated isotopic chains. Although this transition is observed for nuclei exhibiting larger neutron skin thickness, the calculations indicate that it reflects the systematic evolution of nuclear structure, decay energetics, shell effects, fissility, and barrier characteristics rather than the influence of neutron skin thickness alone. Within the present theoretical framework, neutron skin thickness therefore serves as a structural indicator of the underlying evolution of the nuclear system, providing a useful parameter for interpreting systematic trends without acting as an independent determinant of the calculated decay properties.

The systematic behaviours identified in Table 1 are examined in greater detail through the analyses presented in Figures 1-7. These figures provide complementary insight into the relationships among decay energetics, barrier penetrability, spontaneous-fission barrier heights, fissility, and neutron skin thickness, thereby establishing the physical mechanisms governing the competition between cluster decay and spontaneous fission in neutron-rich superheavy nuclei.

Table 1: Comparison of Cluster decay and Spontaneous fission using Conventional approach

Parent nucleus	**Neutron skin thickness (fm)**	**Cluster decay**				**Spontaneous fission**			
		Q-value (MeV)	**Barrier penetrability, (P)**	**Half-life, ($T_{1/2}$) (s)**	**Decay probability, (λ_c) (s^{-1})**	**Q-value (MeV)**	**Barrier height, (B_f) (MeV)**	**Half-life, ($T_{1/2}^{SF}$) (s)**	**Decay probability, (λ_{SF}) (s^{-1})**
260Lr	0.157	31.29	5.6737×10^{-22}	1.1915×10^{0}	5.8174×10^{-1}	222.2	5.036	1.1910×10^{2}	5.8190×10^{-3}
262Lr	0.162	30.95	2.5416×10^{-22}	2.6801×10^{0}	2.5863×10^{-1}	223.64	5.013	2.2330×10^{2}	3.1050×10^{-3}
264Lr	0.168	30.40	6.2715×10^{-23}	1.0983×10^{1}	6.3111×10^{-2}	225.08	4.989	4.1190×10^{2}	1.6830×10^{-3}
262Rf	0.155	44.51	3.9212×10^{-23}	1.5588×10^{1}	4.4467×10^{-2}	223.64	4.997	1.9100×10^{1}	3.6290×10^{-2}
264Rf	0.161	43.42	4.0816×10^{-24}	1.5195×10^{2}	4.5617×10^{-3}	225.08	4.973	3.5900×10^{1}	1.9310×10^{-2}
266Rf	0.166	41.88	1.3212×10^{-2}	4.7901×10^{3}	1.4470×10^{-4}	226.52	4.950	6.6440×10^{1}	1.0430×10^{-2}
266Db	0.159	54.79	8.2579×10^{-28}	7.5666×10^{5}	9.1606×10^{-7}	226.52	4.934	5.7720×10^{0}	1.2010×10^{-1}
268Db	0.165	53.54	6.2119×10^{-29}	1.0198×10^{7}	6.7969×10^{-8}	227.96	4.910	1.0710×10^{1}	6.4720×10^{-2}
270Db	0.170	56.24	2.2776×10^{-26}	2.7197×10^{4}	2.5486×10^{-5}	229.4	4.887	1.9570×10^{1}	3.5410×10^{-2}
270Sg	0.163	69.97	9.7690×10^{-28}	6.2707×10^{5}	1.1054×10^{-6}	229.4	4.871	1.7260×10^{0}	4.0160×10^{-1}
272Sg	0.169	67.78	1.7270×10^{-29}	3.6118×10^{7}	1.9191×10^{-8}	230.84	4.847	3.1630×10^{0}	2.1910×10^{-1}
274Sg	0.174	65.00	6.8270×10^{-32}	9.3506×10^{9}	7.4129×10^{-11}	232.28	4.823	5.7120×10^{0}	1.2130×10^{-1}
274Bh	0.167	75.01	5.8175×10^{-36}	1.1086×10^{14}	6.2525×10^{-15}	232.28	4.808	5.1100×10^{-1}	1.3560×10^{0}
276Bh	0.172	80.20	2.1237×10^{-31}	2.9434×10^{9}	2.3547×10^{-10}	233.72	4.784	9.2540×10^{-1}	7.4900×10^{-1}
278Bh	0.177	88.71	4.9154×10^{-25}	1.2118×10^{3}	5.7198×10^{-4}	235.16	4.759	1.6520×10^{0}	4.1960×10^{-1}
278Hs	0.171	99.92	8.6175×10^{-28}	6.9840×10^{5}	9.9248×10^{-7}	235.16	4.744	1.4990×10^{-1}	4.6250×10^{0}
280Hs	0.176	92.05	2.0366×10^{-33}	3.0858×10^{11}	2.2462×10^{-12}	236.6	4.720	2.6830×10^{-1}	2.5840×10^{0}
282Hs	0.181	98.57	1.5305×10^{-28}	3.9771×10^{6}	1.7429×10^{-7}	238.04	4.695	4.7350×10^{-1}	1.4640×10^{0}
282Mt	0.174	119.50	7.4527×10^{-25}	7.8813×10^{2}	8.7950×10^{-4}	238.04	4.681	4.3550×10^{-2}	1.5920×10^{1}
284Mt	0.179	131.52	1.5809×10^{-18}	3.5497×10^{-4}	1.9527×10^{3}	239.48	4.656	7.7090×10^{-2}	8.9910×10^{0}
286Mt	0.184	95.23	3.9519×10^{-42}	1.6725×10^{20}	4.1444×10^{-21}	240.92	4.631	1.3460×10^{-1}	5.1500×10^{0}
286Ds	0.178	126.04	1.4039×10^{-29}	4.3167×10^{7}	1.6057×10^{-8}	240.92	4.617	1.2540×10^{-2}	5.5250×10^{1}
288Ds	0.182	119.72	1.3030×10^{-33}	4.7834×10^{11}	1.4490×10^{-12}	242.36	4.592	2.1970×10^{-2}	3.1550×10^{1}
290Ds	0.187	128.98	1.3105×10^{-27}	4.5924×10^{5}	1.5093×10^{-6}	243.8	4.567	3.7960×10^{-2}	1.8260×10^{1}
290Rg	0.181	148.25	5.8664×10^{-25}	1.0034×10^{3}	6.9080×10^{-4}	243.8	4.552	3.5840×10^{-3}	1.9340×10^{2}
292Rg	0.186	138.26	1.7716×10^{-30}	3.4486×10^{8}	2.0098×10^{-9}	245.24	4.527	6.2100×10^{-3}	1.1160×10^{2}
294Rg	0.190	156.80	1.4224×10^{-20}	4.0428×10^{-2}	1.7145×10^{1}	246.68	4.502	1.0620×10^{-2}	6.5250×10^{1}
294Cn	0.184	167.76	3.0657×10^{-22}	1.8922×10^{0}	3.6621×10^{-1}	246.68	4.488	1.0150×10^{-3}	6.8260×10^{2}
296Cn	0.189	148.45	2.0506×10^{-32}	3.0144×10^{10}	2.2995×10^{-11}	248.12	4.463	1.7420×10^{-3}	3.9790×10^{2}
298Cn	0.193	157.73	4.9644×10^{-27}	1.2108×10^{5}	5.7247×10^{-6}	249.56	4.437	2.9510×10^{-3}	2.3490×10^{2}
298Nh	0.187	162.83	1.0507×10^{-31}	5.8509×10^{9}	1.1847×10^{-10}	249.56	4.423	2.8550×10^{-4}	2.4270×10^{3}
300Nh	0.192	167.22	3.7669×10^{-29}	1.6143×10^{7}	4.2938×10^{-8}	251	4.398	4.8510×10^{-4}	1.4290×10^{3}
302Nh	0.196	177.40	6.9172×10^{-24}	8.5555×10^{1}	8.1018×10^{-3}	252.44	4.372	8.1390×10^{-4}	8.5170×10^{2}
302Fl	0.191	187.28	1.2904×10^{-25}	4.6223×10^{3}	1.4996×10^{-4}	252.44	4.359	7.9700×10^{-5}	8.6970×10^{3}
304Fl	0.195	187.41	1.9231×10^{-25}	3.1079×10^{3}	2.2303×10^{-4}	253.88	4.333	1.3410×10^{-4}	5.1680×10^{3}
306Fl	0.199	170.71	3.3677×10^{-34}	1.8640×10^{12}	3.7186×10^{-13}	255.32	4.307	2.2300×10^{-4}	3.1090×10^{3}
306Mc	0.194	207.36	2.8480×10^{-22}	2.0647×10^{0}	$3.3560\times10^{-}$)	255.32	4.294	2.2090×10^{-5}	3.1380×10^{4}
308Mc	0.198	186.53	3.0304×10^{-32}	2.0509×10^{10}	3.3797×10^{-11}	256.76	4.268	3.6830×10^{-5}	1.8820×10^{4}
310Mc	0.202	179.71	5.2803×10^{-36}	1.2021×10^{14}	5.7661×10^{-15}	258.2	4.242	6.0680×10^{-5}	1.1420×10^{4}
310Lv	0.196	179.09	7.9925×10^{-44}	8.1912×10^{21}	8.4621×10^{-23}	258.2	4.228	6.0800×10^{-6}	1.1400×10^{5}
312Lv	0.201	192.42	1.6237×10^{-35}	3.8995×10^{13}	1.7775×10^{-14}	259.64	4.202	1.0050×10^{-5}	6.8990×10^{4}
314Lv	0.205	183.61	1.1601×10^{-40}	5.6007×10^{18}	1.2376×10^{-19}	261.08	4.176	1.6410×10^{-5}	4.2230×10^{4}
314Ts	0.199	223.31	7.7826×10^{-26}	7.7768×10^{3}	8.9120×10^{-5}	261.08	4.163	1.6620×10^{-6}	4.1700×10^{5}
316Ts	0.204	191.01	4.4103×10^{-43}	1.4876×10^{21}	4.6595×10^{-22}	262.52	4.137	2.7240×10^{-6}	2.5450×10^{5}
318Ts	0.208	191.69	1.5961×10^{-42}	4.1132×10^{20}	1.6852×10^{-21}	263.96	4.111	4.4120×10^{-6}	1.5710×10^{5}
318Og	0.202	211.85	3.4974×10^{-37}	1.8305×10^{15}	3.7867×10^{-16}	263.96	4.098	4.5170×10^{-7}	1.5350×10^{6}
320Og	0.206	206.06	2.1606×10^{-40}	3.0121×10^{18}	2.3012×10^{-19}	265.4	4.071	7.3390×10^{-7}	9.4450×10^{5}
322Og	0.210	205.77	1.9577×10^{-40}	3.3349×10^{18}	2.0785×10^{-19}	266.84	4.045	1.1790×10^{-6}	5.8790×10^{5}

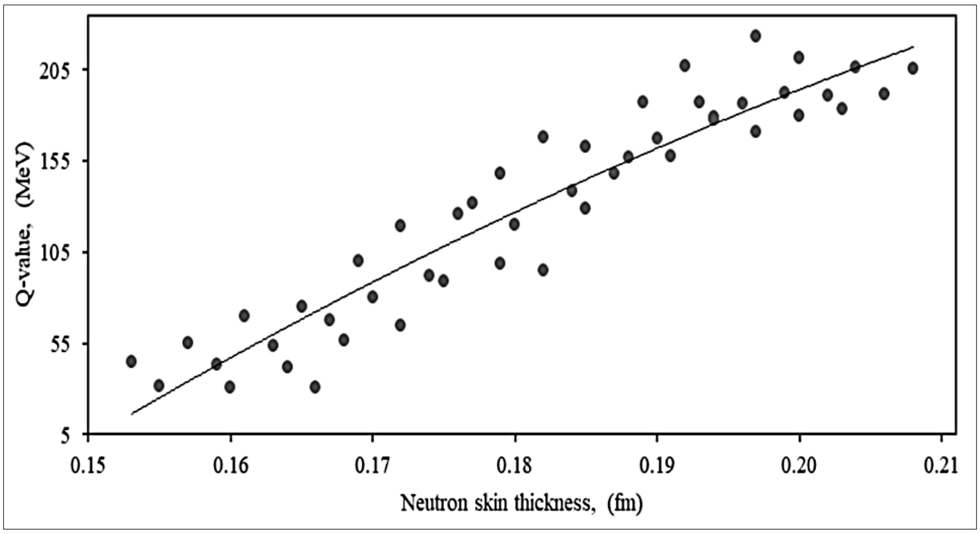

Fig 1: Variation of Q-value with neutron skin thickness using the conventional approach

Figure 1 illustrates that the calculated decay Q-values generally increase with neutron skin thickness. This trend reflects the systematic evolution of nuclear binding energies with increasing neutron excess in superheavy nuclei, where the symmetry-energy contribution modifies the binding-energy balance. The scatter about the overall trend indicates that the calculated Q-values are also influenced by shell structure, nuclear masses, and daughter-nucleus stability. Consequently, the observed behaviour reflects the interplay of nuclear binding and structural effects rather than neutron skin thickness alone.

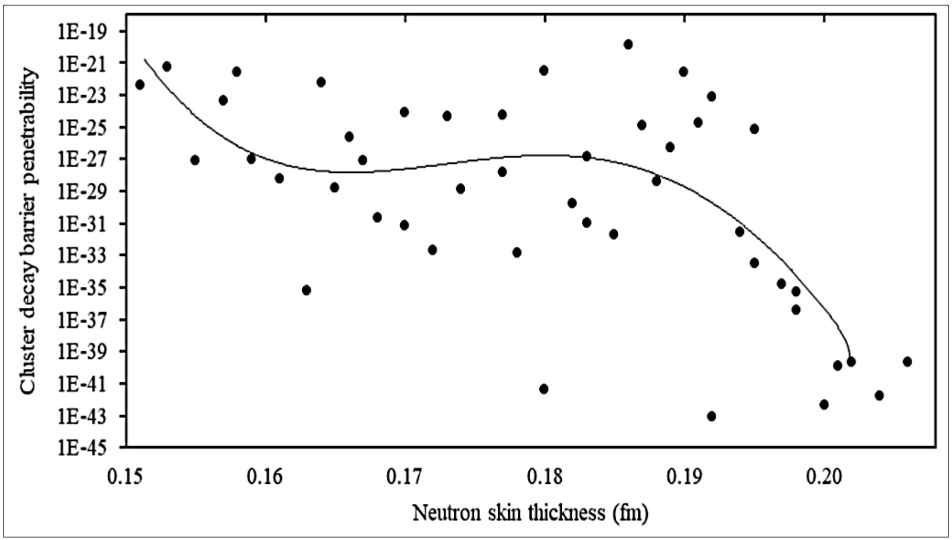

Fig 2: Relationship between cluster decay barrier penetrability and neutron skin thickness in the conventional approach

As shown in Figure 2, the calculated cluster-decay barrier penetrability generally decreases with increasing neutron skin thickness. Within the WKB framework, a larger effective nuclear radius increases the tunnelling distance, thereby reducing the probability of barrier penetration. The dispersion of the calculated values further indicates that penetrability depends on the decay Q-value, emitted-cluster charge, reduced mass, interaction potential, and shell effects. These results demonstrate that barrier penetrability is governed by the combined influence of barrier characteristics and nuclear structure.

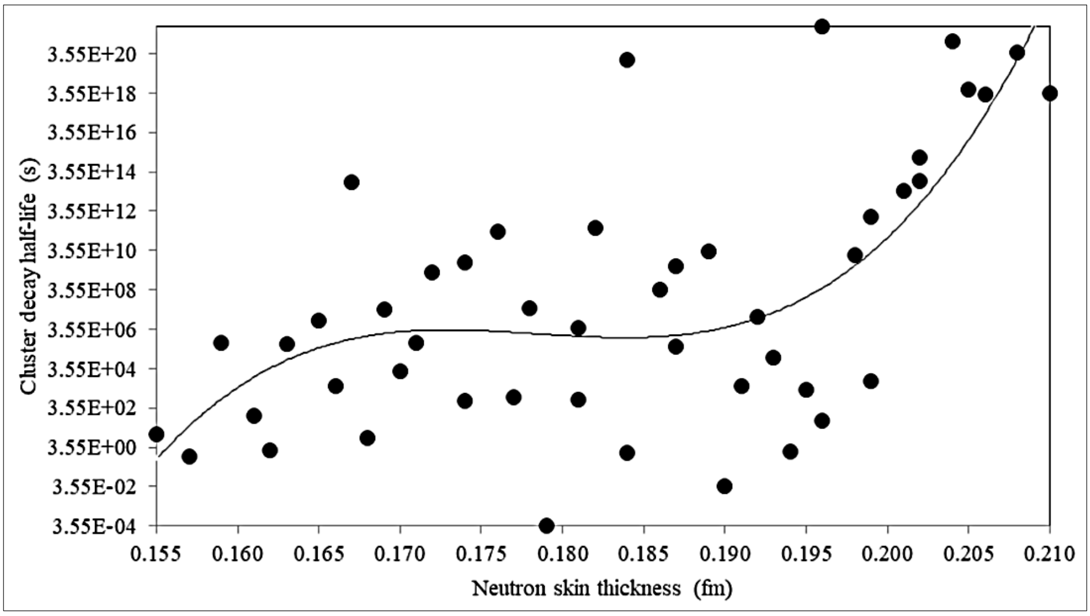

Fig 3: Dependence of cluster decay half-life on neutron skin thickness based on the conventional approach

Figure 3 shows that the calculated cluster-decay half-lives increase with neutron skin thickness. This behaviour follows directly from the reduction in barrier penetrability, which decreases the decay constant and consequently increases the half-life. The spread of the calculated values indicates that neutron skin thickness alone does not determine the cluster-decay lifetime. Instead, the half-life is controlled by the decay Q-value, emitted-cluster properties, reduced mass, Coulomb interaction, shell stabilization, cluster preformation, and barrier penetrability.

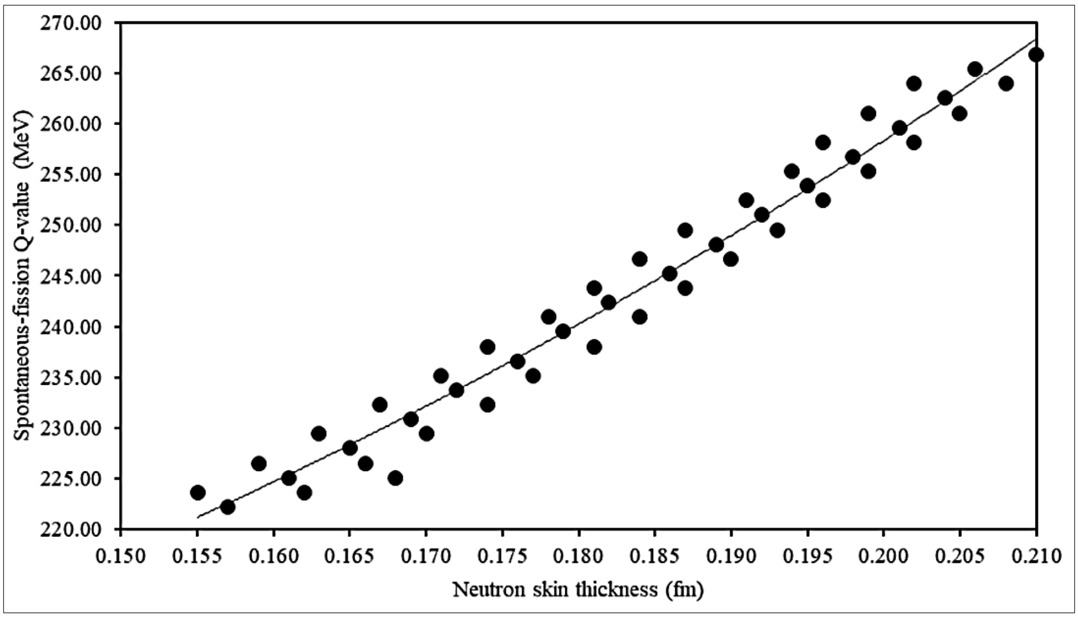

Fig 4: Variation of spontaneous fission Q-value with neutron skin thickness under the conventional approach

The calculated spontaneous-fission Q-values shown in Figure 4 generally increase with neutron skin thickness, reflecting the evolution of nuclear masses and binding-energy differences across the investigated isotopic chains. The observed scatter indicates that the energy release is additionally influenced by shell effects, pairing correlations, fragment configurations, mass asymmetry, and the binding energies of the parent nucleus and fission fragments. Within the present framework, neutron skin thickness serves as a structural indicator of these systematic variations rather than an independent determinant of the calculated spontaneous-fission Q-values.

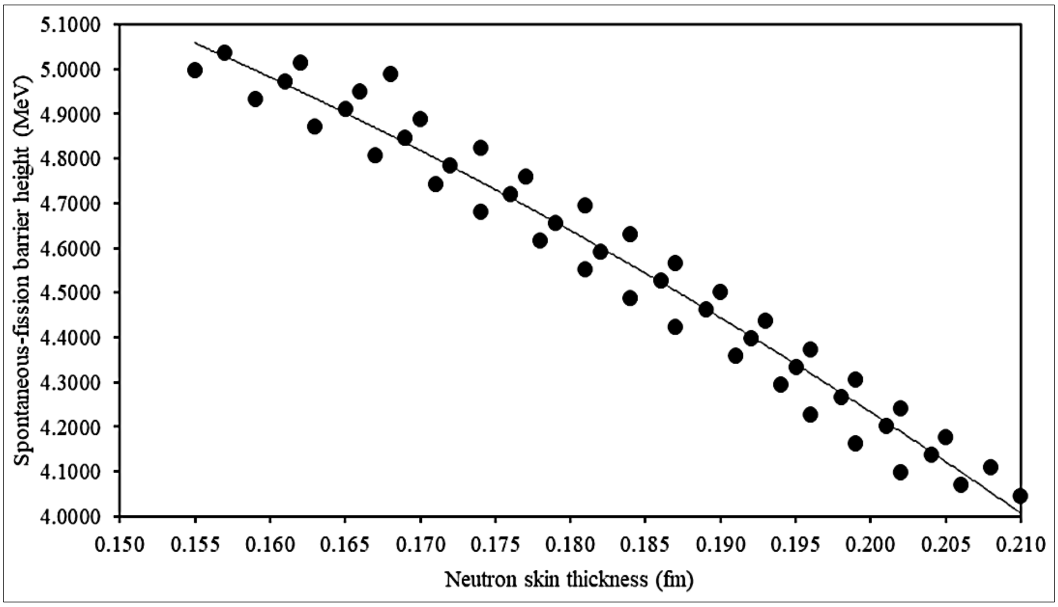

Fig 5: Relationship between spontaneous fission barrier height and neutron skin thickness using the conventional approach

Figure 5 demonstrates that the calculated spontaneous-fission barrier heights decrease progressively across the investigated nuclei. This behaviour results from increasing fissility and stronger Coulomb repulsion in heavier superheavy nuclei, which reduce the resistance to collective deformation despite the increasing neutron skin thickness. Consequently, lower barrier heights enhance spontaneous-fission probability and strengthen its competition with cluster decay.

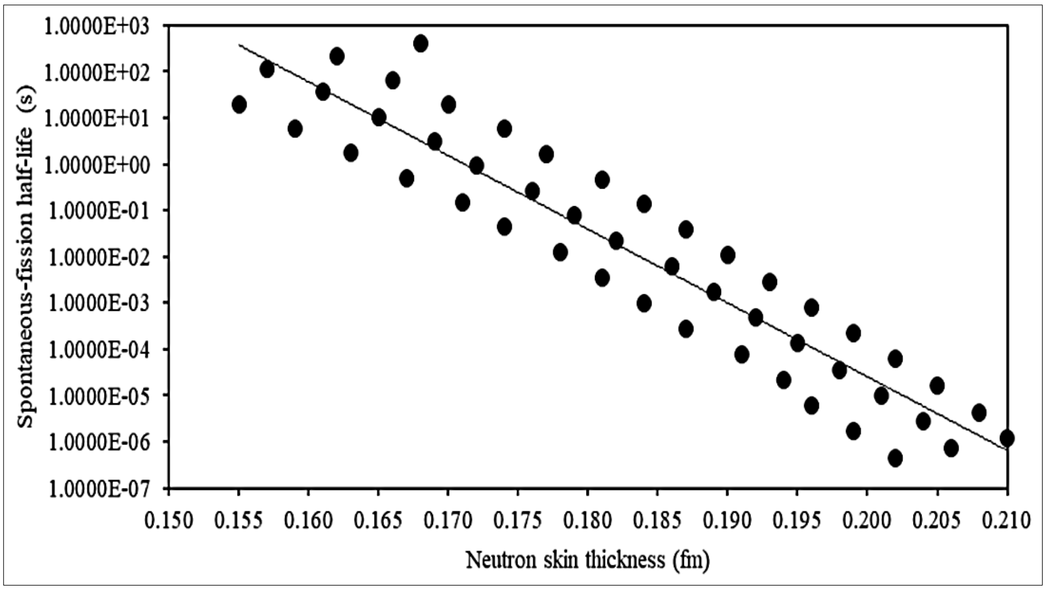

Fig 6: Dependence of spontaneous fission half-life on neutron skin thickness in the conventional approach

As illustrated in Figure 6, the calculated spontaneous-fission half-lives decrease systematically with increasing neutron skin thickness. This trend follows from the progressive reduction in fission-barrier height, which enhances quantum tunnelling through the deformation barrier. The scatter of the calculated values indicates that spontaneous-fission half-life is also influenced by barrier characteristics, shell effects, deformation, pairing correlations, and fissility. The calculated results therefore remain consistent with the established relationship between barrier height and spontaneous-fission probability.

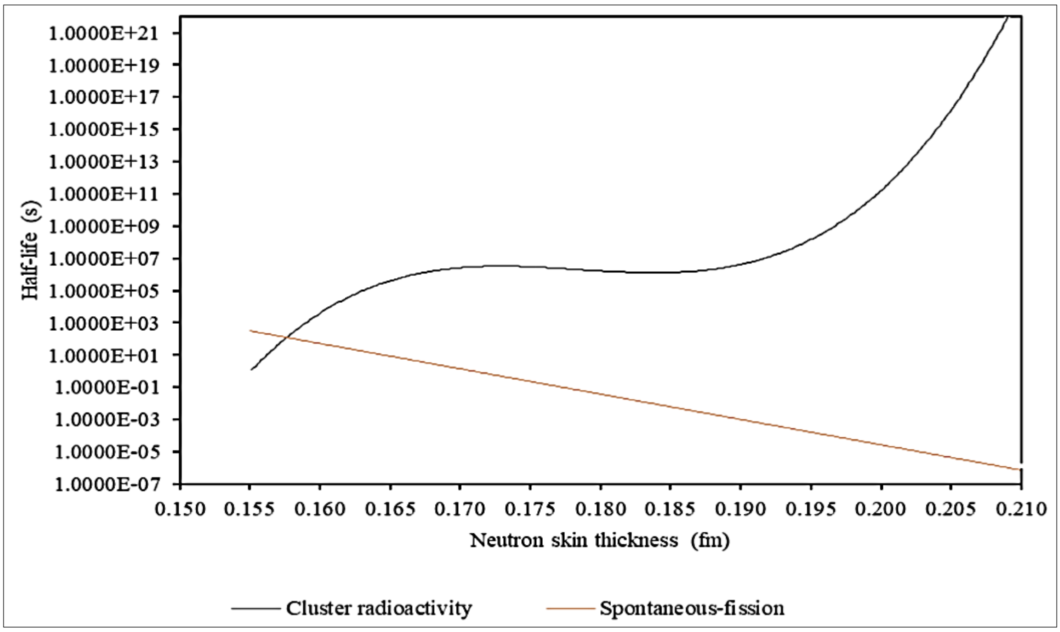

Fig 7: Conventional approach Comparative variation of cluster radioactivity and spontaneous fission half-lives with neutron skin thickness

Figure 7 compares the calculated cluster-decay and spontaneous-fission half-lives across the investigated isotopic chains. At smaller neutron skin thicknesses, cluster decay exhibits shorter half-lives and therefore higher decay probabilities than spontaneous fission. With increasing neutron skin thickness, cluster-decay half-lives become progressively longer because of reduced barrier penetrability, whereas spontaneous-fission half-lives decrease as the fission barrier is lowered. Consequently, a transition from cluster-decay dominance to spontaneous-fission dominance is observed. This transition reflects the systematic evolution of decay energetics, barrier properties, shell effects, and fissility across the investigated nuclei. Although it occurs for nuclei with larger neutron skin thickness, the present calculations indicate that neutron skin thickness functions as a structural indicator of these underlying changes rather than an independent determinant of the preferred decay mode. The identified transition provides valuable insight into the decay behaviour and stability of neutron-rich superheavy nuclei.

Table 2 shows the comparison between Spontaneous fission half-life results of conventional approach for a sample of the selected elements and the experimental data available in the NUBASE2020 decay data. The calculated spontaneous-fission half-lives are compared with the available experimental data from NUBASE2020 for representative superheavy nuclei. The conventional approach yields a root-mean-square (RMS) deviation of 1.822, indicating satisfactory agreement with experiment. The remaining deviations are consistent with the inherent challenges of describing shell effects, deformation, pairing correlations, and fission-barrier properties in superheavy nuclei. Overall, the comparison demonstrates that the present framework captures the principal systematics governing spontaneous-fission half-lives while providing reliable benchmark predictions for neutron-rich superheavy systems.

Table 2: Comparison of Spontaneous fission half-lives of Conventional approach with available NUBASE2020 experimental data

Parent nucleus	Experimental half-life (s)	Conventional approach Half-life (s)
260Lr	1.80×10^{2}	1.1910×10^{2}
262Lr	1.44×10^{4}	2.2330×10^{2}
264Lr	3.6×10^{4}	4.1190×10^{2}
262Rf	2.5×10^{-1}	1.9100×10^{1}
264Rf	3.6×10^{3}	3.5900×10^{1}
266Rf	1.44×10^{4}	6.6440×10^{1}
266Db	4.8×10^{3}	5.7720×10^{0}
278Bh	2.0×10^{0}	1.6520×10^{0}
278Hs	2.0×10^{0}	1.4990×10^{-1}

Conclusion

The density-dependent cluster model combined with the Wentzel-Kramers-Brillouin (WKB) approximation was employed to investigate the competition between cluster decay and spontaneous fission in selected superheavy nuclei with atomic number Z>103. The calculated results demonstrate that cluster decay is governed primarily by the combined effects of decay Q-values, barrier penetrability, shell stabilization, daughter-nucleus configurations, and emitted-cluster properties, whereas spontaneous fission is controlled predominantly by the systematic reduction of fission-barrier heights with increasing fissility and Coulomb repulsion.

A transition from cluster-decay dominance to spontaneous-fission dominance is identified across the investigated isotopic chains. Although this transition is observed for nuclei exhibiting larger neutron skin thickness, the calculated results indicate that it reflects the systematic evolution of nuclear structure, decay energetics, shell effects, and barrier characteristics, with neutron skin thickness serving as a structural indicator rather than an independent determinant of the calculated decay properties.

Comparison with the available experimental spontaneous-fission half-lives yields a root-mean-square deviation of 1.822, demonstrating satisfactory agreement between the calculated and measured values. Overall, the present study provides a systematic assessment of competing decay modes in superheavy nuclei and establishes benchmark predictions for future theoretical investigations of neutron-rich superheavy systems. Future theoretical developments should explicitly incorporate neutron skin thickness into the interaction potential and barrier formulation to systematically evaluate its influence on decay characteristics, nuclear stability, and the interpretation of newly synthesized neutron-rich superheavy nuclei within more comprehensive theoretical frameworks.

Acknowledgments

The authors gratefully acknowledge the Department of Physics, University of Eldoret, for providing the academic environment and institutional support that facilitated this research.

References

1. Alamanos N, Borge MJG, Hofmann S, Möller P, Popeko AG. Heavy and super-heavy nuclei and elements: production and properties. Eur Phys J A. 2025;61(1):3. DOI:10.1140/epja/s10050-024-01468-3
2. Zagrebaev V, Karpov A, Greiner W. Possibilities for synthesis of new superheavy nuclei in fusion reactions. J Phys G Nucl Part Phys. 2011;39(1):015106. DOI:10.1088/0954-3899/39/1/015106
3. Zagrebaev VI, Karpov AV, Mishustin IN, Greiner W. Superheavies: theoretical incitements and predictions. Phys Rev C. 2011;83(4):044618. DOI:10.1103/PhysRevC.83.044618
4. Zhang MH, Zhang ZY, Gan ZG, Zhou SG, Zhang FS. Progress on the synthesis of superheavy nuclei. Nucl Sci Tech. 2025;36(12):204. DOI:10.1007/s41365-025-01781-6
5. Blendowske R, Fliessbach T, Walliser H. The preformation of clusters in heavy nuclei. Z Phys A. 1988;329(2):121-125. DOI:10.1007/BF01289567
6. Krane KS. Introductory Nuclear Physics. John Wiley & Sons; 1988.
7. Poenaru DN, Gherghescu RA, Greiner W. Heavy-particle radioactivities of superheavy nuclei. Phys Rev C. 2011;83(1):014601. DOI:10.1103/PhysRevC.83.014601
8. Gamow G. Zur Quantentheorie des Atomkernes. Z Phys. 1928;51(3-4):204-212. DOI:10.1007/BF01343196
9. Wentzel G. Eine Verallgemeinerung der Quantenbedingungen für die Zwecke der Wellenmechanik. Z Phys. 1926;38(6-7):518-529. DOI:10.1007/BF01397171
10. Kramers HA. Wellenmechanik und halbzahlige Quantisierung. Z Phys. 1926;39(10-11):828-840. DOI:10.1007/BF01451751
11. Brillouin L. La mécanique ondulatoire de Schrödinger; une méthode générale de résolution par approximations successive. C R Acad Sci. 1926;183:24-26.
12. Landau LD, Lifshitz EM. Quantum Mechanics: Non-Relativistic Theory. 3rd ed. Pergamon Press; 1977.
13. Griffiths DJ, Schroeter DF. Introduction to Quantum Mechanics. 3rd ed. Cambridge University Press; 2018.
14. Liu J, Wang Z, Zhang H, Ren Z. Theoretical predictions on cluster radioactivity of superheavy nuclei with Z=119,120. Chin Phys C. 2024;48(1):014105. DOI:10.1088/1674-1137/ad0827
15. Wang Z, Ren Z. Exploring α-decay chains and cluster radioactivities of superheavy $^{293-295}$119 isotopes. Eur Phys J A. 2024;60(3):74. DOI:10.1140/epja/s10050-024-01301-x
16. Saxena G, Akrawy DT, Ahmed AH, Aggarwal M. Theoretical investigation of heavy cluster decay from Z=118 and 120 isotopes: a search for an empirical formula in superheavy region. Nucl Phys A. 2024;1046:122867. DOI:10.1016/j.nuclphysa.2024.122867
17. Ismail M, Abd-Elnasser SG, Adel A, Abdul-Magead IAM, Elsharkawy HM. Systematic investigation of α- and cluster decay modes in superheavy nuclei. Phys Rev C. 2024;109(1):014606. DOI:10.1103/PhysRevC.109.014606
18. Ismail M, Adel A, Ibrahim A. Improved unified formulas for α-decay and cluster radioactivity in heavy and superheavy nuclei: effects of daughter-nucleus deformation. Eur Phys J A. 2025;61(11):259. DOI:10.1140/epja/s10050-025-01723-1
19. Jain D. Exploring cluster radioactivity and decay half-lives using different density distributions. Phys Rev C. 2025;111(6):064603. DOI:10.1103/PhysRevC.111.064603
20. Saxena G, Sharma PK, Saxena P. A global study of α-clusters decay in heavy and superheavy nuclei with half-life and preformation factor. Eur Phys J A. 2024;60(2):50. DOI:10.1140/epja/s10050-024-01227-4
21. Swiatecki WJ. Systematics of spontaneous fission half-lives. Phys Rev. 1955;100(3):937-938. DOI:10.1103/PhysRev.100.937
22. Myers WD, Swiatecki WJ. Nuclear masses and deformations. Nucl Phys. 1966;81(1):1-60. DOI:10.1016/0029-5582(66)90639-0
23. Royer G. Alpha emission and spontaneous fission through quasi-molecular shapes. J Phys G Nucl Part Phys. 2000;26(8):1149-1170. DOI:10.1088/0954-3899/26/8/305
24. Cameron AGW. A revised semi-empirical mass formula. Can J Phys. 1957;35(10):1021-1031. DOI:10.1139/p57-080
25. Blanco H, Giuliani SA, Rodríguez-Guzmán R, Robledo LM. Spontaneous fission lifetimes from microscopic approaches. Atoms. 2023;11(1):23. DOI:10.3390/atoms11010023
26. Blanco JM, Dobrowolski A, Zdeb A, Bartel J. Spontaneous fission half-lives of actinides and superheavy elements. Phys Rev C. 2023;108(4):044618. DOI:10.1103/PhysRevC.108.044618
27. Chai QZ, Wang JL, Liu XH. Effects of triaxial deformation on the fission barrier in the Z=118-120 nuclei. Commun Theor Phys. 2024;76(6):065301. DOI:10.1088/1572-9494/ad3b8e
28. Bezbakh AN, Rahmatinejad A, Adamian GG, Antonenko NV. Dependencies of the fission path of superheavy nuclei on the excitation energy and spin-orbit strength. Phys Rev C. 2026;113(4):044609. DOI:10.1103/35rl-vpmq
29. Yuan Z, Bai D, Wang Z, Ren Z. Improved formulas of spontaneous fission half-lives for heavy and superheavy nuclei. Eur Phys J A. 2024;60(3):68. DOI:10.1140/epja/s10050-024-01280-z
30. Moiseev NS, Antonenko NV, Adamian GG. Empirical systematics of spontaneous fission half-lives of heavy and superheavy nuclei. Phys Rev C. 2025;112(3):034607. DOI:10.1103/qv5w-2c9g
31. Xie Y, Wang N, Ren Z. Spontaneous fission half-lives for heavy and super-heavy nuclei from phenomenological

models. Preprint. Posted online December 22, 2025. DOI:10.48550/arXiv.2512.21453
32. Wang W, Ma N, Zhang Y, Wei Z, Zhang H. Competition of decay modes for Z=119 and Z=120 superheavy nuclei. Eur Phys J A. 2024;60(11):226. DOI:10.1140/epja/s10050-024-01444-x
33. Sandhu K, Kaur G, Sharma MK. Investigation of heavy particle radioactivity and spontaneous fission of even-Z superheavy nuclei. Chin Phys C. 2025;49(4):044102. DOI:10.1088/1674-1137/ada126
34. Jain A, Sharma PK, Jain SK, Akrawy DT, Saxena G. Decay properties of undetected superheavy nuclei with Z>110. Preprint. Posted online June 19, 2023. DOI:10.48550/arXiv.2306.11581
35. Brown BA. Neutron radii in nuclei and the neutron equation of state. Phys Rev Lett. 2000;85(25):5296-5299. DOI:10.1103/PhysRevLett.85.5296
36. Centelles M, Roca-Maza X, Viñas X, Warda M. Origin of the neutron skin thickness of ^{208}Pb in nuclear mean-field models. Phys Rev Lett. 2009;102(12):122502. DOI:10.1103/PhysRevLett.102.122502
37. Warda M, Viñas X, Roca-Maza X, Centelles M. Neutron skin thickness in the droplet model with surface width dependence: indications of softness of the nuclear symmetry energy. Phys Rev C. 2009;80(2):024316. DOI:10.1103/PhysRevC.80.024316
38. Burgio GF, Das HC, Vidaña I. The nuclear symmetry energy and the neutron skin thickness in nuclei. Front Astron Space Sci. 2024;11:1505560. DOI:10.3389/fspas.2024.1505560
39. Ding MQ, Fang DQ, Ma YG. Neutron skin and its effects in heavy-ion collisions. Nucl Sci Tech. 2024;35(12):211. DOI:10.1007/s41365-024-01584-1
40. Tanaka M, Horiuchi W, Fukuda M. Unveiling radii and neutron skins of unstable atomic nuclei via nuclear collisions. Front Phys. 2024;12:1488428. DOI:10.3389/fphy.2024.1488428
41. Seif WM, Sargsyan VV, Adamian GG, Antonenko NV. Influences of isospin-asymmetry and skin thickness on fusion of oxygen isotopes at stellar energies. Phys Rev C. 2024;109(3):034604. DOI:10.1103/PhysRevC.109.034604
42. Audi G, Kondev FG, Wang M, Huang WJ, Naimi S. The NUBASE2020 evaluation of nuclear properties. Chin Phys C. 2021;45(3):030001. DOI:10.1088/1674-1137/abddae
43. Wang M, Huang WJ, Kondev FG, Audi G, Naimi S. The AME2020 atomic mass evaluation (II). Tables, graphs and references. Chin Phys C. 2021;45(3):030003. DOI:10.1088/1674-1137/abddaf